$(H_2O)_6$ on a Virtual Metal Surface: Testing the Surface Ice Rules

Timm Lankau*

Institut für Physikalische Chemie, University of Hamburg, 20146 Hamburg, Germany

Ian L. Cooper

Department of Chemistry, University of Newcastle upon Tyne, Newcastle upon Tyne NE1 7RU, United Kingdom

Received: October 2, 2000; In Final Form: January 8, 2001

The water hexamer has been studied with a classical water−water interaction potential and by quantum calculation at both RHF and MP2 levels. The influence of a virtual metal surface on $(H_2O)_6$ has been modeled through geometry constraints on the cluster. Additional data on $(H_2O)_2$ and $(H_2O)_3$ are presented to assist the interpretation of the results obtained for the hexamer. These calculations suggest that water molecules in the first layer with their hydrogens pointing away from the surface ('flip up') only occur for a small range of values of surface lattice constants. In all other cases, the dipole moment of the water molecules is found to lie nearly parallel to the metal surface.

1. Introduction

The problem of the orientation of hydrogen atoms in the first layer of water molecules is fundamental to studies of the water−metal systems. Experiments suggest that the hydrogen atoms in the layer of water adjacent to the metal surface either point slightly upward into the following water layers as expected for water bound to metal via the oxygen lone pair[1] or lie parallel to the metal surface.[2,3] [The words "up" and "down", "bottom" and "top", respectively, are used in the following sense: The metal surface is defined as the foundation of the platinum−water−vacuum interface. The water bilayer resting on this surface consists of the two layers, a "lower" layer bound directly to the metal surface and a "top" layer at the vacuum−water interface.] Theoretical calculations, on the other hand, are unable to unambiguously determine the orientation of the hydrogen atoms, because the water molecule orientation depends strongly on cluster size and the chosen method of calculation.[4] An extensive review of water-metal interactions has been given by Thiel and Madey.[1]

Early work[5,6] on the adsorption of water on Pt(111) reported a $(\sqrt{3} \times \sqrt{3})$ R30° surface structure of adsorbed water molecules and suggested the formation of ice ordered in domains of 30−40 Å in length.

A water bilayer structure[1,7] has been proposed as the basis of the growth of ice on hexagonal metal latices. The structure of this water bilayer is generally explained in terms of an extension to surfaces[7] of the Bernal−Fowler−Pauling rules (ice rules).[8,9] Specifically,[7] each water molecule is bound by at least two bonds (which may be hydrogen bonds to other water molecules or oxygen lone pair bonds to the surface) while maintaining a tetrahedral configuration. Each water molecule in the lower layer closest to the metal surface is bound to the surface via a lone pair orbital on the oxygen, and all free lone pair orbitals on oxygen remain nearly perpendicular to the surface. In an ideal infinite bilayer, all water molecules have their dipole moments pointing away from the surface ("flip up"), whereas in a finite cluster, water molecules whose dipole moments point toward the surface ("flip down") may occur at the edge of the cluster.[7,10,11] Doering and Madey,[7] using the surface-extended ice-rule set, concluded that the smallest stable water cluster on a hexagonal metal surface should be the water nonamer. Such an $(H_2O)_9$ cluster has been observed on Ru-(0001) within an $(6\sqrt{3} \times 6\sqrt{3})$ R0° superstructure,[7,12] whereas experiments suggest that the smallest cluster possible on platinum(111) is a three-dimensional water trimer.[13]

The metal−water interface has been examined previously by quantum calculations,[14−27] and work on the platinum−water interface[14−18] suggests that the molecular plane of the water lies parallel to the surface.[4,14−16] These results agree with work function measurements[2,13,28,29] on water-covered platinum surfaces, which show that a contribution of about 0.2 D of the water dipole moment (single molecule 1.84 D) lies normal to surface.[2] Theory and experiment agree that the water molecule is only slightly distorted upon adsorption on Pt(111),[2,10,13,29−33] and dissociation has only been observed experimentally on precovered surfaces.[34−37]

The extension to surfaces[7] of the ice rules[8,9] assumes a continuous transition between water directly attached to the surface and crystalline ice. On the other hand, experiment and theory suggest that the surface of an ice crystal has a different structure than that of the bulk. Snowflakes have been reported to be covered by a quasiliquid layer (QLL), with a higher density than ice.[38,39] Molecular dynamics simulation[40] of an ice crystal suggests the existence of molten ice on the crystal surface below the freezing point of water, and scanning tunneling microscopy (STM)[14] provides evidence for three solid and one liquid ice phase on platinum(111). Morgenstern et al. concluded from their STM experiments that the fourth liquid 2 D water phase on Pt(111) has a higher density than the solid 2D ice phases observed in three-dimensional water and ice. Dosch et al.[39] suggest that the formation of a QLL can be induced by a surface-induced distortion of the hydrogen bonding network and LEED

* To whom correspondence should be addressed. E-mail: lankau@chemie.uni-hamburg.de.

10.1021/jp0035986 CCC: $20.00
Published on Web 04/03/2001

experiments of ultrathin water films on Pt(111) suggest a disordered ice layer.[3]

The link between water adsorption on metal surfaces at low coverages and extended ice layers is formed via water clusters on a metal surface and in a vacuum. The water dimer, the most widely analyzed water cluster, is not only the first water cluster to be treated by ab initio calculations[41] but is also commonly used as a benchmark test for new calculations, including nearly every possible level of theory.[42−71] The global minimum corresponds to a linear geometry with C_S symmetry in which the nonbonding hydrogen atoms lie on opposite sites of the oxygen−oxygen bond. The optimized oxygen−oxygen distance is around 2.95 Å, and the binding energy is around 5.0 kcal/mol according to high level quantum chemical calculations[68,69] (A review of the water dimer is provided in ref 70 and recently in ref 71).

Schütz et al. have proposed a scheme for referring to the nonbonding hydrogen atoms in the cyclic water trimer, which fully describes the geometry of the cluster:[72] The nonbonding hydrogen can be either above (up, "u"), parallel to (planar, "p"), or under (down, "d") the plane of oxygen atoms, whereas the bonding hydrogens lie in the plane of the oxygen atoms. When this plane bisects a water molecule, the geometry is marked with a "b". The global minimum of the potential-energy surface of the water trimer corresponds to a ring structure. Early calculations suggested that the {uuu} water trimer is less stable and the {ppp} trimer is more stable than the ideal linear structure.[73] The linear trimer transforms smoothly into a {uud} ring structure,[4] which defines the global minimum.[46,63,72,74−85] The geometry of the water trimer is flexible, and tunneling facilitates rapid changes among the 96 ($2^n \times n! \times 2$, where n is the number of water molecules) isoenergetic isomers in the cluster.[85−91]

The potential-energy surface of the water trimer[82−83] is found to display 18 stationary points. The {ppp} trimer has a slightly smaller binding energy than the {uud} trimer ($\Delta^{\{ppp\}}_{\{uud\}}E_{TRIM} <$ 0.5 kcal/mol)[4,72] and is a stationary point with a Hessian index of 3. Most calculations relate to the {uud} trimer, and only a few treat the {ppp} trimer,[72,80−82,92−94] despite the fact that the {ppp} and {udp} trimers form possible intermediates in the rearrangement of the hydrogen atoms.[72]

The computational analysis of water clusters has gained interest recently, because such microcrystals can be used to investigate phase transitions.[95] However, the transition from small to large water clusters is not straightforward, and the water hexamer separates two types of clusters.

The structure of water clusters is characterized by the number of hydrogen bonds, being a maximum, and repulsive interactions between nonbonding hydrogens and geometrical strains within the water rings, being simultaneously a minimum. Small water clusters ($(H_2O)_n$ with $n \leq 5$) are therefore commonly assumed to be cyclic and planar,[63,73,87,96−102] whereas larger clusters with $n \geq 7$ have three-dimensional structures.[95,103−110] The water hexamer delineates these regimes and is the smallest water cluster with a three-dimensional equilibrium structure.[111] Several stable geometries with similar energies ($\Delta_{HEX}E <$ 1 kcal/mol) have been found for the water hexamer.[63,78,79,112−115] The multitude of energetically similar isomers makes the water hexamer a benchmark system for those methods to be applied to larger clusters.

Although the cyclic water hexamer forms the basis of the ice structure[116] and has been observed as a structural element in liquid water,[117] the most stable water hexamer in the gas phase has a cage structure.[118,119] The energy difference between the cyclic hexamer and the cage hexamer is small, and the free hexamer has been observed experimentally only recently.[119]

Quantum calculations[63,78,79,112−115,120] on the cyclic water hexamer are in reasonable agreement regarding geometry but disagree on energy. The most stable ring has a "chair" conformation (S_6 symmetry) with linear hydrogen bonds and an oxygen−oxygen distance between nearest neighbors which varies between 2.708 and 2.855 Å. The geometrical features of the cluster can be reproduced by simple treatments, whereas reliable energy calculations require more sophisticated treatments. With one exception (66.66 kcal/mol[115]), published values for the binding energy of the cyclic water hexamer vary between 37.99 and 56.00 kcal/mol depending on the level of computation.[63,78,79,112−114,120]

Structural elements of the water dimer and trimer can be observed within the water hexamer. Because a description of the water hexamer is facilitated by reference to these structures, we include here a summary of our results for $(H_2O)_2$ in section 3 and $(H_2O)_3$ in section 4. Section 5, which concentrates on the water hexamer, has been subdivided into subsections for clarity. Subsection 5.1 describes the geometry of the water hexamer and describes the computational model. This complements section 2 which summarizes the computational methods applied in general to all water clusters. Subsection 5.2 describes the free hexamer and subsection 5.3 considers the imposition of geometrical constraints on the water hexamer to simulate a virtual metal surface, independent of the nature of the metal. In subsection 5.4, the surface constant of the virtual surface is varied systematically, allowing us to correlate the orientation of the hydrogen atoms close to the surface with the geometry of the interface. Subsection 5.5 considers the water hexamer as part of an ice bilayer and relates our results to experiment. A summary is included as section 6.

2. Computational Procedure

The classical analysis of water clusters is based on a water−water interaction potential similar to that of Kistenmacher and Popkie.[49,50] The water molecule has a rigid geometry based on experimental data, with an OH bond length of 0.9572 Å and an HOH bond angle of 104.52°, whereas the center of negative charge M (−1.40 e) lies 0.24 Å along the symmetry axis toward the hydrogens.[121]

In addition to the Coulomb forces, the repulsive forces between the atoms are taken into account. Equation 1 summarizes (in atomic units) the potentials between the different centers on the water molecules, where M denotes to the center of the negative charge. The positive charges are located at the positions of the hydrogen atoms.

$$V_{HH} = \frac{fq^2}{4r} + a_1 e^{-b_1 r} \qquad V_{OH} = a_2 e^{-b_2 r} \qquad V_{HM} = \frac{-fq^2}{2r}$$

$$V_{MM} = \frac{fq^2}{r} \quad (1)$$

The original parameters of Kistenmacher and Popkie were optimized to reproduce the results of a set of quantum calculations (GAMESS UK,[122] DZP basis set,[123] MP3, full BSSE counterpoise correction of Boys and Bernadi[124]) for 120 dimers and four trimers.[4] During parameter optimization, a higher weight was placed on the trimers so as to partially include cooperative effects into the new force field. These new parameters (Table 1) are used entirely in this work. [During optimization of the force field parameters, the contribution of the oxygen−oxygen repulsion to the binding energy of the

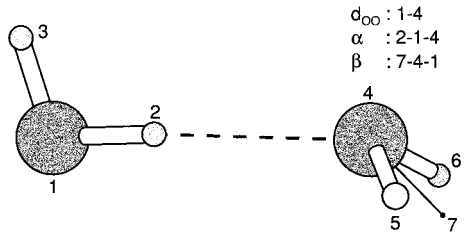

Figure 1. Water dimer.

TABLE 1: Water−Water Interaction Parameters

parameter	value
r_{OH} (Å)	0.9572
$\angle_{HOH}$ (degrees)	104.52
r_{OM} (Å)	0.2382
q (e)	−1.398 323
a_1 (kcal mol^{-1})	653.7789
a_2 (kcal mol^{-1})	3457.857
b_1 (Å^{-1})	3.189 600
b_2 (Å^{-1})	3.545 410
f (kcal Å mol^{-1} e^{-2})	332.177 52

TABLE 2: Calculated Properties of the Water Dimer

	r_{OO} [Å]	α [degrees]	β [degrees]	$-E_{DIM}$ [kcal mol^{-1}]
Pot	2.9834	8.55	123.40	4.903
MP3[a]	2.9926	2.44	135.47	4.914
MP3	2.9354	3.28	125.43	5.949
MP2	2.9116	3.79	124.06	6.282
RHF	2.9921	1.99	132.03	5.131
experiment[b]	2.98 ± 0.04	0 ± 10	120 ± 10	5.4 ± 0.7
[68]	2.953	6.8	124	5.05

[a] BSSE corrected. [b] References 43, 137, and 138.

clusters was found to be negligible close to equilibrium geometries, whereas a strong oxygen−hydrogen repulsion was necessary to avoid physically unrealistic structures. Therefore, our classical potential does not contain an oxygen−oxygen repulsion term. Currently we are investigating the importance of the oxygen−oxygen repulsion for water clusters at geometries far from equilibrium.[4]]

The quantum calculations were performed at the same fixed geometry as the classical calculations. For these calculations we used Gaussian 94[125] with the DZP basis set[3] at HF and MP2 levels, without BSSE correction. [GAMES UK uses six Cartesian d functions, whereas Gaussian 94 uses five $l = 2$ d functions. The difference in results using these basis sets was found to be negligible.]

In our model, we assume the water hexamer to be constructed from water molecules rather than from individual atoms, so that interaction energies relate in general to molecular interactions. Where interaction energies between selected atoms are required in the analysis of the water hexamer, these interaction energies are explicitly indicated.

3. Water Dimer

Figure 1 displays the most stable water dimer, and Table 2 displays its geometrical parameters calculated at various levels of theory. With the introduction of electron correlation, the oxygen−oxygen distance decreases ($\Delta_{HF}^{MP2} r_{OO} = -0.0805$ Å) and the hydrogen bond becomes stronger ($\Delta_{HF}^{MP2} E_{DIM} = -1.151$ kcal/mol). As the level of correlation increases from MP2 to MP3, the length of the hydrogen bond increases ($\Delta_{MP2}^{MP3} r_{OO} = +0.0238$ Å) and the binding energy is reduced ($\Delta_{MP2}^{MP3} E_{DIM} = +0.333$ kcal/mol). The MP2 approach appears to overestimate electron correlation, whereas MP3 appears to compensate for this effect.[70] Finally, a full BSSE correction was applied to the binding energy and the geometry. The BSSE in the geometry was eliminated manually. A fine mesh of points was calculated with a BSSE corrected energy around the MP3 optimal geometry, and the minimum of this energy surface was computed numerically. The BSSE correction produces an extended oxygen−oxygen distance ($\Delta_{MP3}^{BSSE} r_{OO} = +0.0572$ Å) and reduces the binding energy ($\Delta_{MP3}^{BSSE} E_{DIM} = +1.035$ kcal/mol). Because of the BSSE correction, the oxygen−oxygen distance is longer and the binding energy is lower than the corresponding HF values. The figure of −5 kcal/mol for E_{DIM} appears reasonable, because our calculations with other basis sets and a full BSSE correction also yielded binding energies of about −5 kcal/mol at all levels of theory. Furthermore, large scale calculations on the water dimer by Klopper et al. reported BSSE-corrected interaction energies below −5 kcal/mol.[80]

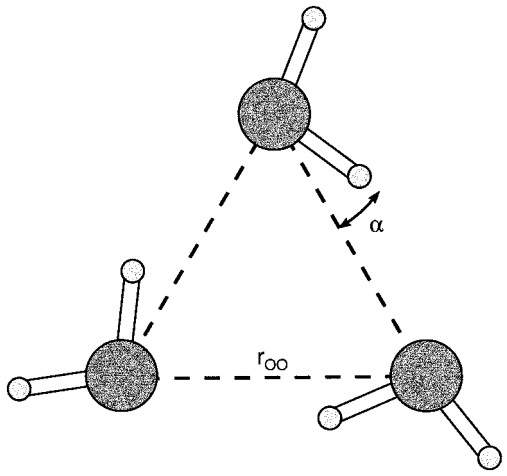

Figure 2. C_{3h} Water trimer.

The BSSE-corrected values agree well both with experiment and with earlier quantum calculations ($r_{OO} = 2.73-3.04$ Å, α = −7.2° to +5.1°, $\beta = 150-120°$, $-E_{DIM} = 3.6-7.2$ kcal/mol, $-E_{DIM} = 3.7-5.0$ kcal/mol BSSE corrected).[43−60,62,63,70] The BSSE-corrected MP3 data were used to generate a classical water−water interaction potential applicable to the analysis of small water clusters at equilibrium geometry, because calculations with previously published classical interaction potentials yielded similar geometries but high binding energies (5.7−7.2 kcal/mol).[64−67] The classical potential calculations reproduce the quantum results (MP3, BSSE corrected) reasonably well: r_{OO} is reduced ($\Delta_{MP3}^{Pot} r_{OO} = -0.0092$ Å), whereas the binding energy is well reproduced ($\Delta_{MP3}^{Pot} E_{DIM} = -0.011$ kcal/mol). Only the bending angle of the new hydrogen bond (α = 8.55°) is larger than the calculated quantum result, following the inclusion of the trimers into the optimization of the force field parameters, but is still in reasonable agreement with the experiment.

4. Water Trimer

Figure 2 displays the planar water trimer with C_{3h} symmetry and Table 3 indicates the geometrical parameters and binding energy calculated at various levels of theory. A BSSE correction to the trimer geometry at MP3 level was not carried out because of the computational effort required.

The predicted oxygen−oxygen distance r_{OO} is shorter than that in the dimer in all cases. Even the classical potential calculation shows a reduction in bond length of 2.4%, close to

TABLE 3: Calculated Properties of the Planar {ppp} Water Trimer

	r_{OO} [Å]	α [degrees]	$-E_{TRIM}$ [kcal mol^{-1}]
Pot	2.9135	24.18	13.685
MP3	2.8014	23.54	16.213[a]
MP2	2.7782	23.55	17.020
RHF	2.8830	23.27	13.916

[a] BSSE corrected 13.789 kcal mol^{-1}.

that found at Hartree−Fock level (2.9%). A similar result has been obtained for other trimers with various geometries.

These results show that the shortening of the bonds arises from cooperative effects in the water cluster. In the planar {ppp} trimer, such interactions account for 21% of the total (BSSE corrected) energy. The classical potential does not contain terms which take cooperative effects directly into account, but the bonds are still shorter than in the free dimer. This reduction is caused through interaction with the second nearest neighbor in the cluster. These energies are generally more strongly binding than in the quantum calculations. Repulsive interactions with the second nearest neighbor were reduced by 78% in the classical calculation, whereas attractive interactions were increased by 26%. Interactions between nearest neighbors are similar in both the quantum and classical calculations. For a fixed hydrogen bond geometry, these energies differ by about 0.9%. The second nearest neighbor interactions in the classical model tend to reproduce attractive many-body forces reasonably well but give poorer results for repulsive forces.

The angle α of the hydrogen bond was found to be similar at all levels of theory (about 23°), suggesting that stable water clusters are possible with severely distorted hydrogen bonds. A positive value for the coupling constant between r_{OO} and α (classical potential: $\partial^2 E_{TRIM}/(\partial\alpha\ \partial d_{OO}) = 0.44$ kcal mol^{-1} deg^{-1} Å^{-1}) indicates that as r_{OO} increases, α tends to zero, and the bonding hydrogen atom lies on the line joining the two oxygen atoms.

The classical energy of formation of the trimer (E_{TRIM}) is smaller than the MP3 result, but the BSSE correction to the MP3 energy (−13.789 kcal/mol) shows that the classical calculation matches the binding energy for the planar water trimer reasonably well.

The value of E_{TRIM} (−13.685 kcal/mol) for the {ppp} trimer is close to that found at the global minimum (−14.035 kcal/mol) using the classical potential. This global minimum has C_1 symmetry and {uud} geometry. The two hydrogen atoms which point upward move out of plane (dihedral angle HOOH = 23°), reducing their repulsion.

Our quantum results for the {ppp} water trimer are in reasonable agreement with previously published values (r_{OO} = 2.80−2.88 Å, α = 20−25°, $-E_{TRIM}$ = 13.0 and 16.7 kcal/mol),[72,80−82,92−94] [the last three being optimized with a fixed value for r_{OO}]. Xantheas and Dunning[77] and van Duijneveldt-van de Ridjt and van Duijneveldt[81] reported three-body terms of about 2.3 and 2.0 kcal/mol for the global minimum structure (C_1 symmetry) of the water trimer, whereas Del Bene and Pople[48] found a value of 2.94 kcal/mol for the planar trimer, which is in close agreement with our results (2.87 kcal/mol).

Cooperative effects have a significant effect on the structure of the water trimer at the quantum level. Our classical calculations indicate that both a reduction in repulsive forces between nonbonding hydrogen atoms and interaction between second nearest neighbor water molecules are critical to the geometry of the trimer when calculated with a classical potential.

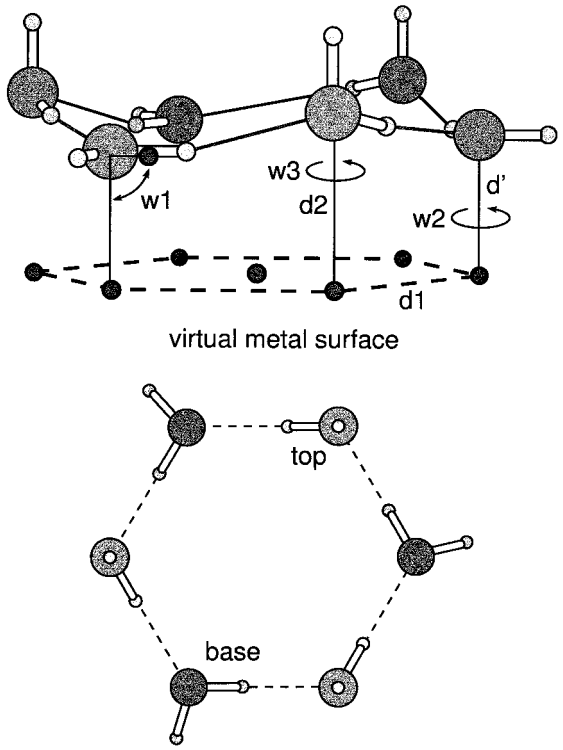

Figure 3. Water hexamer on the virtual surface (d1 = 2.8 Å): (a) sideview. (b) topview.

5. Water Hexamer

5.1. The Model. The structure of the metal−water interface is dominated both by the interaction between the surface atoms and the water molecules in the first layer and by the interactions among the water molecules within the ice cluster. To distinguish between these two effects, the surface was replaced by a mesh of auxiliary geometrical points and the water cluster was maintained close to the ideal bilayer geometry proposed by Doering and Madey.[7] The platinum−water bond was assumed to have the same geometry as that expected for a Lewis acid−base bond between the oxygen lone pair and the surface atom as the starting point for the geometry optimization. The influence of the surface on the water hexamer is solely described by geometrical constraints and no other electronic effects of the surface are included in the model. Use of the water hexamer as a model for the bilayer structure allows us to study the influence of geometrical constraints on the bilayer structure as water adsorbs on to the surface independently of the nature of the surface.

Figure 3a shows the water hexamer bound to a virtual metal surface and an identification of its geometrical parameters. A hexagonal mesh of seven auxiliary geometrical points (d1 is the unit length of the mesh.) was placed below the cluster to model the metal surface. The water hexamer is assumed to have the same structure as a six-membered water ring in the ideal infinite bilayer structure. Each water molecule rests on top of a virtual metal atom/auxiliary point. The water molecules in the first layer (base plane) are assumed to lie at a fixed distance (d' = 1 Å) from the virtual surface, while the distance d2 between the virtual surface and a second layer water molecule (top plane) is allowed to vary during the calculations. The difference, h = d2 − d', is a measure of the nonplanarity of the oxygen ring.

Both hydrogen atoms associated with a water molecule in the base plane lie the same distance from the surface, with one hydrogen being used to form the hydrogen bond to the top plane. The angle w1 between the bond to the virtual surface and the

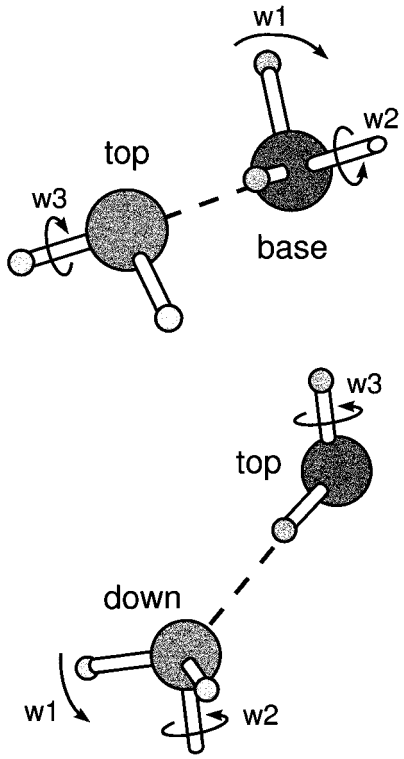

Figure 4. Water dimers in the surface-constrained hexamer. The arrows indicate the direction of motion as w1 decreases, w2 increases, and w3 increases. (a) Base→top water dimer. (b) Top→base water dimer.

molecular plane of the water molecule is allowed to vary during geometry optimization so as to compensate for different heights (d2) of the ring or to break the surface−oxygen bond via the lone electron pair if necessary.

The water molecules in the base plane are also allowed to rotate around their bond to the virtual metal surface (w2). This rotation is required to describe the interaction between second nearest neighbors, because it allows the water molecules to form new hydrogen bonds.

One hydrogen−oxygen bond in the top plane water of molecules is initially chosen perpendicular to the virtual metal surface (see section 5.3), whereas the second is used for the hydrogen bond to the base plane. This arrangement, following from the surface ice rules, simulates the interaction to the next water layer in an extended ice cluster. A water molecule in the top layer is allowed to rotate around the bond to the virtual surface (w3) and has two degrees of freedom, as does a water molecule in the base plane. The angles w1−w3 are defined with respect to the symmetry axis of the water molecule and an auxiliary point, which lies between the hydrogen atoms (Figure 3a).

Figure 3b shows a topview of the water hexamer. The oxygen−oxygen bonds lie on top of the metal−metal bonds. This hexagon (dotted line in Figure 3b) designates the ideal orientation of a hydrogen bond. As the angles w2 and w3 are allowed to vary during geometry optimization, the bonding hydrogen atom can deviate from this ideal direction (Figure 4). For values of w2 > −52° or w3 > −60°, the bonding hydrogen atoms lie within the hexagon. Rotations around the surface−oxygen bond, which result in one of these values, are described as 'inward'.

Because the hexagonal symmetry of the surface is not allowed to change during the calculations, each surface is defined by the surface lattice constant d1. Different metal surfaces may be simulated by variation of the geometrical constraint imposed by d1.

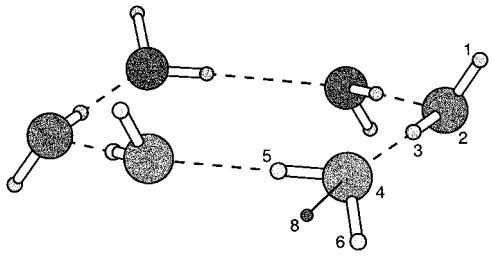

Figure 5. Free water hexamer. Point 8 lies of the C_2 axis of the water molecule; h is the distance between the oxygen triangles. r_{OO}, 2−3; α, 3−2−4; β, 8−4−2; γ, 180°, − ∠(8−4−2−1).

5.2. The Free Water Hexamer. We summarize here for completeness results for the free water hexamer (Table 4) before considering how this structure is affected by the presence of the virtual metal surface. Geometry optimization of the free water hexamer (Figure 5) using the classical potential yields a structure comprising six nearly ideal hydrogen bonds (E_{DIM} = −4.774 kcal/mol): the oxygen−oxygen distance (2.9539 Å) is smaller than in the dimer (2.9834 Å) but larger than in the trimer (2.9135 Å); the hydrogen atoms are located on the oxygen−oxygen line (α = 0.57°); the angle β of 148.89° between the molecular plane of the hydrogen acceptor and the oxygen−oxygen bond is larger than in the dimer (Figure 1, Table 2); and the bond itself is slightly twisted, with γ = 11.42° (ideal value γ = 0°).

The strong bonds between nearest neighbors ($\sum E_{DIM}^{1st}$ = −28.644 kcal/mol) account for 81% of the total energy (−35.397 kcal/mol), and the interactions between second nearest neighbors ($\sum E_{DIM}^{2nd}$) account for an additional 14%. Both the geometry and the energy of formation appear to be determined by these forces.

The geometry optimization of the free water hexamer via quantum calculation (DZP/MP2) resulted in a similar structure: The hydrogen bonds were nearly linear (α = 2.54°) but, as expected, shorter (2.73 Å), in agreement with that reported by Tsai and Jordan (2.725 Å)[114] and Xantheas (2.714 Å).[79] The binding energy of −53.75 kcal/mol reproduces that found by Mhin et al. (−53.94 kcal/mol, MP2/DZP HF optimized geometry)[113] and is close to that of Kim and Kim (−56.00 kcal/mol, MP2/DZP).[112]

We conclude that the results obtained with the classical potential for the water hexamer are reasonably accurate, although they produce systematically an extended oxygen−oxygen separation.

5.3. The Constrained Hexamer. In calculations of the water hexamer on a virtual surface (e.g., for Pt(111), d1 = 2.77 Å), the hydrogen bonds of the hexamer lie directly above the metal−metal bonds of the virtual surface, as shown in Figure 3. Following geometry optimization, the binding energy of the hexamer was lowered by 2.754 kcal/mol. The interactions between nearest and second nearest neighbor molecules account for 95.2% of the total energy (−32.643 kcal/mol). Analysis of the binding energy calculated with the classical potential shows that the energies of the direct hydrogen bonds (top→base and base→top; Figure 4) differ by 0.337 kcal/mol and are generally weaker ($\Delta_{surf}^{free} E_{DIM}^{1st}$ = 0.464 kcal/mol) as the symmetry changes from S_6 to C_3. This weakening can be accounted for by an increase in repulsion between the hydrogen atoms, which is partially compensated by an increase in interaction between second nearest neighbors (E_{DIM}^{2nd}) of 2%, accounting for the relief of stress necessary to compensate for mechanical distortions induced by the surface.

The water hexamer under surface conditions was slightly more nonplanar than the free one ($\Delta^{surf}_{free}h = 0.18$ Å); the base hydrogen atoms were slightly tilted toward the surface (w1 = 89.17°), whereas the oxygen−oxygen distance was reduced (2.8665 Å) from that observed in the free hexamer. To check whether this result arose as an artifact of the chosen input geometry, the calculations were repeated with fewer geometrical constraints.

Geometrical constraints on the water cluster were lifted except that the hydrogen atoms of the base water molecule remained at the same height from the surface and the oxygen atoms were placed at the corners of the virtual metal hexagon (d1 = 2.77 Å). On geometry optimization, the total energy was lowered by about 0.362 kcal/mol, but the water cluster retained its basic shape. The base hydrogens moved slightly upward (Δw1 = 4.32°) as the ring became nonplanar ($\Delta h = 0.078$ Å). The nonbonding hydrogen atoms of the top water molecules moved slightly from the vertical axis (7.03° measured between the vertical and the OH bond of the top hydrogen), still allowing for the formation of an ice cluster, whereas both types of bonding hydrogen atoms (base→top and top→base hydrogen bonds) moved outside the virtual metal hexagon (w2 = −52.3°, w3 = −65.17°).

The rearrangement of the nonbonding hydrogens in the top layer is in agreement with the surface ice rules, which require these hydrogens to lie nearly perpendicular to the metal surface. The nonbonding top hydrogen atoms point slightly into the hexagon and form the basis for epitaxial growth of further ice layers. With each additional water layer the ring contracts until finally the bulk value for ice Ih is reached (d1 = 2.6 Å). This would imply that, with increasing water coverage, a single water molecule should become more strongly bound to the water cluster already on the surface. Ogasawara et al.[126] observed a high-temperature shift of the ice peak on Pt(111) with increasing water coverage in their TDS (temperature controlled desorption spectroscopy) experiment. They suggested this shift to be due to zero-order desorption kinetics and to further stabilization of water in the ice overlayer. This stabilization may be correlated with the orientation of the nonbonding hydrogens at the top of the water hexamer observed here.

Brudermann et al.[127] concluded from their He atom scattering from large water clusters that the water molecules become more strongly bound with increasing cluster size. Supported by theoretical calculations, they argue that the strain in the hydrogen bond network in small clusters reduces the {O−O−O} bending force constant. Our calculations suggest that a similar effect should apply to water clusters on Pt(111) where the strain in the hydrogen bond network is induced by the surface and becomes smaller as the cluster grows in size.

To confirm the physical relevance of such data the calculations of the second step above were repeated at MP2 level. The energy necessary to constrain the free water hexamer at the surface was similar (MP2, 4.3 kcal/mol; Pot, 2.7 kcal/mol) and in both sets of calculations the hydrogens of the base water molecules pointed toward the virtual surface (w1 MP2, 83.5°; Pot, 89.2°). In addition, the oxygen−oxygen bond lengths were in reasonable agreement (MP2, 2.78 Å; Pot, 2.87 Å).

5.4. Variation of the Surface Lattice Constant. Our calculations suggest that the water molecules in the first layer on a metal surface such as Pt(111) can lie parallel to the surface and that the growth of ice crystals remains possible. Calculations were repeated for various values of the surface lattice constant d1. For d1 = 2.77 Å [Pt(111)], the orientation of the nonbonding top hydrogen atoms has only a minor influence on total energy (1% of the total energy −33.005 kcal/mol). In the following calculations, these hydrogens were constrained to lie vertically for convenience, but the water molecules were still allowed to rotate around the bond to the virtual metal surface.

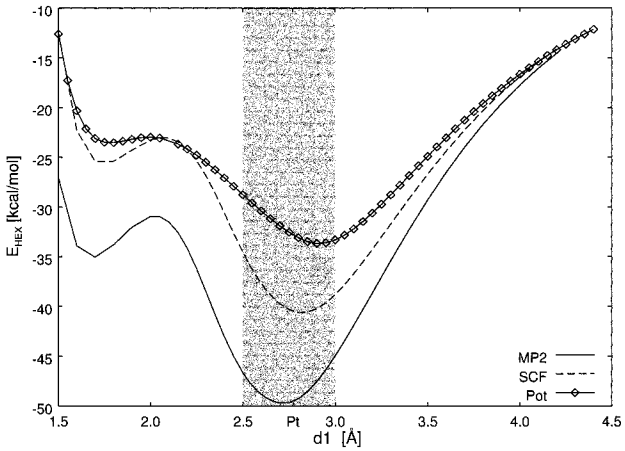

Figure 6. Energy of formation E_{HEX} of the water hexamer under surface constraints.

TABLE 4: Calculated Properties of the Free Water Hexamer (S_6 symmetry)

	r_{OO} [Å]	α [degrees]	β [degrees]	γ [degrees]	h [Å]	E_{HEX} [kcal mol^{-1}]
Pot	2.9535	0.57	148.89	11.42	0.5595	−35.397
RHF	2.8201	3.19	145.78	3.62	0.3135	−44.039
MP2	2.7285	2.54	141.82	0.95	0.2245	−53.747

Figure 6 shows the energy of formation E_{HEX} at various levels of theory as a function of the surface lattice constant d1. The curves are very similar, each displaying two minima. The second, global, minimum represents a distorted water hexamer (Table 5; SCF optimum in Figure 3), whereas the first shallow minimum represents two loosely bound water trimers which dissociate as the value of d1 is further reduced.

Both the binding energy of the hexamer and the oxygen−oxygen distance r_{OO} behave the same as those for the water trimer: With an increasing level of theory, the global minimum moves to smaller values of d1 and corresponds to higher binding energies. As d1 is reduced, the oxygen−oxygen bond length becomes shorter as the ring becomes nonplanar ($\Delta h = 0.05$ Å).

With increasing level of theory, the global minimum of the potential-energy curve moves into the range predicted by Thiel and Madey for the existence of bilayer structures (2.48 Å (Ni) < d1 < 2.89 Å (Ag); gray shaded in Figure 6),[1,128] indicating the formation of icelike water clusters on metal surfaces in agreement with the surface ice rules (see section 5.1). Figure 6 also suggests that the range of suitable surfaces may be larger than predicted.

The formation of water trimers within the hexamer at small values of d1 can be observed in Figure 7, which shows selected pair interaction energies calculated with the classical potential. The strength of the hydrogen bond between nearest neighbors (E^{1st}_{DIM}) decreases as d1 decreases, whereas the strength of the interaction between second nearest neighbors (E^{2nd}_{DIM}) increases. These interactions form the basis for the formation of water trimers, because, as d1 becomes smaller, the hexamer breaks into two trimers. This cleavage eliminates the repulsive forces between the base plane and the top layer, and the total energy of the cluster is controlled by the repulsive forces within the newly formed water trimers.

TABLE 5: Global Minima of the Potential-Energy Curves for the Constrained Water Hexamer (Figure 6)

	d_1 [Å]	d_2 [Å]	r_{OO} [Å]	w_1 [degrees]	w_2 [degrees]	w_3 [degrees]	$-E_{HEX}$ [kcal mol^{-1}]	$-\Delta E_{TOP}$[a] [kcal mol^{-1}]
Pot	2.90	1.44	2.93	80.72	−52.44	−63.24	33.66	10.862
SCF	2.80	1.39	2.83	86.12	−51.97	−64.51	40.59	14.558[b]
MP2	2.70	1.44	2.74	90.78	−52.19	−64.15	49.67	18.199[b]
ideal[c]	2.6	1.9	2.76	125	−52	−60		10.56

[a] Binding energy of a top plane water molecule. [b] Calculated at the global optimum. [c] Approximate values for ice Ih.

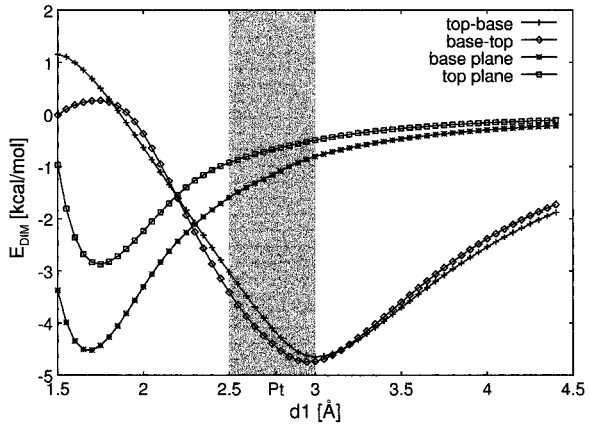

Figure 7. Pair interaction energies E_{DIM} in the water hexamer (classical potential).

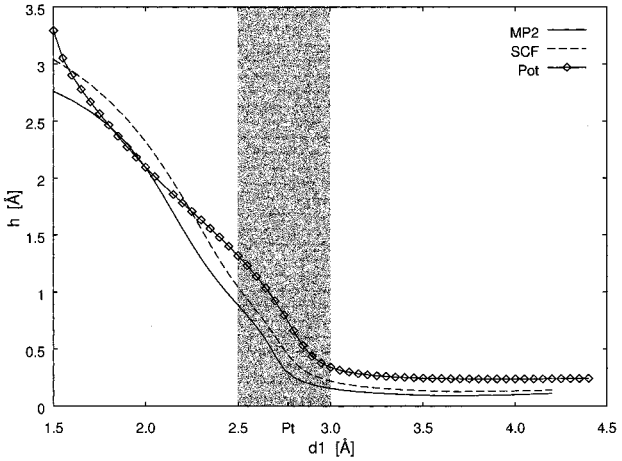

Figure 8. Nonplanarity (h) of ring as function of surface lattice constant d1.

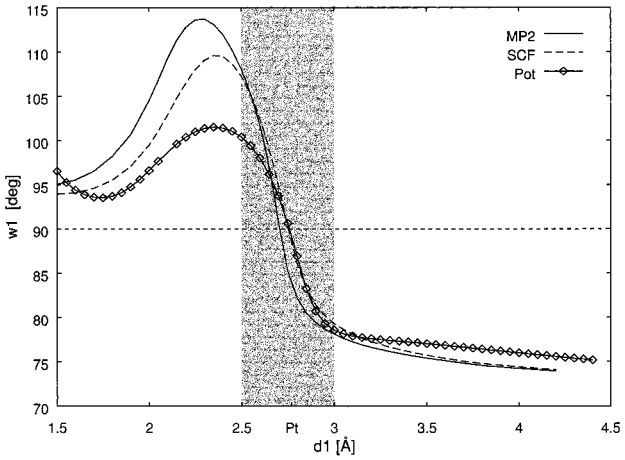

Figure 9. Angle w1 as a function of surface lattice constant d1.

We note that interactions between second nearest neighbors in the base plane are as strong as those between nearest neighbors. These second nearest neighbor interactions influence the geometry of the cluster even at large values of d1. For d1 = 1.7 Å, the total interaction energy between second nearest neighbors (E_{DIM}^{2nd}) in the base plane is 13.56 kcal/mol, a value close to the binding energy of the free {ppp} water trimer (13.68 kcal/mol). In the top plane, the second nearest neighbor interactions are small and are of a shorter range than those in the base plane.

The strength of the hydrogen bond between nearest neighbors does not depend significantly on orientation; a top or a base plane water molecule may donate a hydrogen atom to the bond. Both curves in Figure 7 have similar shapes over the given interval for d1. At large values of d1, the top→base hydrogen bond is slightly more favorable than the base→top hydrogen bond because the former is closer to the optimal hydrogen bond of the free water dimer. In the physically important region (2.5 Å ≤ d1 ≤ 3.0 Å), the base→top hydrogen bond is stronger than the top-base hydrogen bond. Within this range, the basal hydrogen atoms move upward and strengthen the hydrogen bonds.

The maximum in total energy (Figure 6) can be accounted for via Figure 7. The nearest neighbor interactions (E_{DIM}^{1st}) become antibonding more readily than those between second nearest neighbors (E_{DIM}^{2nd}) become bonding, causing a maximum in total energy. The dissociation of the water hexamer is controlled by interactions between nearest and second nearest neighbors.

Figure 7 shows that both the top→base and base→top hydrogen bonds are similar in strength despite their different geometries (Figure 4). Significant differences can be observed only for interactions between second nearest neighbor molecules. These interactions are much stronger in the base plane (E_{MIN}^{2nd} = −4.52 kcal/mol) than in the top plane (E_{MIN}^{2nd} = −2.87 kcal/mol), and this difference has a strong influence on the geometry, because the second nearest neighbor interactions in the base plane contribute significantly to the total energy, whereas contributions in the top layer are negligible over a wide range of values of d1.

Figure 8 displays the nonplanarity of the water ring (h = d2 − d') as a function of d1. Again all three curves display similar features. As d1 is reduced, the ring remains almost planar until around 2.7−3 Å when the nonplanarity increases linearly with d1. A further change, not shown in Figure 8, can be observed for d1 < 1.5 Å, as the hexamer breaks in two trimers.

Within the range of validity of the surface ice rules the water ring is essentially planar. It is therefore probable that the water hexamer lies flat on heavy metal surfaces, and ideal icelike structures (h > 0) can be expected only for values of d1 smaller than 2.6 Å (e.g., Fe, Co, Ni, and Cu[128]).

As the water ring tends to planarity, the hydrogen atoms associated with the base plane move closer to the surface. Figure 9 shows how w1 varies with d1, all three curves showing similar behavior. For values of d1 ≳ 2.7 Å, the hydrogen atoms in the basal water molecules point toward the surface until w1 reaches a constant value of 75°. This motion stabilizes the base→top

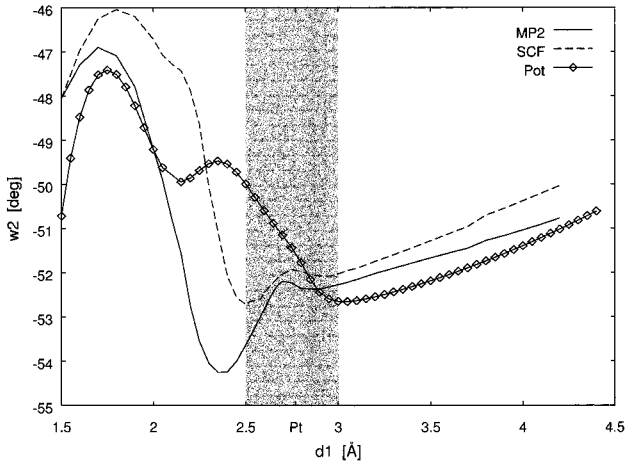

Figure 10. Angle w2 as a function of surface lattice constant d1.

hydrogen bond (Figure 4a), because the geometry of the base→top water dimer approaches the ideal dimer geometry with C_S symmetry (to be compared with the basal plane of the free water hexamer, Figure 5). At a value of 75°, two opposing effects compensate: the hydrogen atoms of the water molecules in the base plane move as far down as possible to reduce repulsion among the nonbonding hydrogen atoms without significantly distorting the base→top hydrogen bond, because the bonding hydrogen atom moves out of its ideal position as w1 decreases.

Values of w1 smaller than 90° are unlikely to be observed in practice, because the water molecule binds to most metal surfaces via a lone pair, and a water molecule oriented such that its hydrogens point downward would require cleavage of the metal−oxygen bond.[4]

For d1 < 2.7 Å, w1 increases to a maximum. In this region, the changes of w1 and d2 are coupled. As the nonplanarity of the ring increases, the basal hydrogen atoms move upward to maintain strong base→top hydrogen bonds. With increasing levels of theory, the maximum value of w1 increases but fails to reach the value of 125.26° applicable to ideal tetrahedra. The closest arises at MP2 level (113.74°), when, at d1 = 2.3 Å, r_{OO} reaches its minimum of 2.64 Å, smaller than the value of 2.76 Å found for the ideal ice structure. The structure closest to the ideal ice structure can be observed only outside the range proposed by Thiel and Madey.

Further reduction in d1 produces a decrease in w1, when the hexamer splits into two trimers. The optimal structure for a trimer in the base plane of the water hexamer is almost planar (d1 = 1.8 Å, r_{OO} = 3.05 Å, α = 25.29°, w1 = 93.70°) when the hydrogen atoms in the basal water molecules move downward to bind to second nearest neighbor water molecules.

The splitting of the hexamer into two trimers can also be inferred from Figure 10 which displays w2 as a function of d1. For w2 > −52°, the bonding hydrogen atoms of the basal water molecules rotate into the water hexagon and point toward second nearest neighbor molecules.

For both small and large values of d1, quantum and classical results for w2 agree except in the central region (Δ^{Pot}_{MP2} w2 ≈ 5°). Figure 7 shows that for d1 ≈ 2.3 Å the interactions between nearest and second nearest neighbors in the base plane are similar in magnitude. At d1 = 3 Å, the interactions between second nearest neighbors contribute 7.2% of the total energy; this contribution increasing rapidly as d1 decreases. Because the interaction between the second nearest neighbors in the base plane increases with w2, the bonding hydrogen atoms of the base molecules turn into the hexagon. This slightly weakens the base→top hydrogen bonds, which are still similar in magnitude to the top→base bonds in this region. The classical potential, which is based on pairwise interactions, cannot compensate for the distortion of the dimer through cooperative effects. To balance the individual hydrogen bonds in the hexamer, the rotation of the base water molecules ceases when d1 equals 2.35 Å and the bonding hydrogens turn back to reinforce the top→base hydrogen bonds until the interactions between second nearest neighbors dominate the total energy. Figure 7 shows how the top→base hydrogen bonds become more favorable than the base→top bonds in this region.

Quantum calculations include cooperative effects, and these effects are likely to compensate for the distortion of hydrogen bonds between nearest neighbors. Artificially high interactions between second nearest neighbors as observed in classical calculations are therefore not necessary to compensate for the distortion. The bonding hydrogen atoms of the base water molecules can move out of the hexagon to form strong top→base dimer bonds, and only for small values of d1 do the hydrogens move back into the hexagon to form trimers.

The first maximum (classical potential d1 = 1.8 Å) in Figure 10 suggests the formation of a planar water trimer (classical potential, r_{OO} = 3.05 Å, α = 25.29°) in the base plane. Both r_{OO} and α are close to their free {ppp} water trimer values (r_{OO} = 2.91 Å, α = 24.18°). The hydrogen bonds in the free C_{3h} water trimer are bent, and the formation of such a trimer on a metal surface is likely for small values of d1. At d1 = 1.75 Å, the binding energy (Figure 6) displays a local minimum, suggesting the formation of a planar trimer in the base plane, in agreement with the maximum in Figure 10.

Calculations on the free water trimer show that, with increasing values of r_{OO}, α becomes smaller and the bonding hydrogen atoms turn back onto the oxygen−oxygen line. Such an effect is not observed in the water hexamer. As d1 increases, the bonding hydrogen atoms move away from the oxygen triangle in the base plane to form hydrogen bonds between nearest neighbor molecules and w2 becomes more negative. The rotation of the bonding hydrogens in the base plane does not cease at −52°, when they move out of the water hexagon to minimize repulsions within the top→base bond (Figure 4b), whereas the base→top hydrogen bond becomes stronger as the bonding hydrogen atoms move into the oxygen−oxygen line (Figure 4a). As d1 increases, the repulsive forces decrease and the bonding hydrogen atoms in the basal water molecules turn back toward the oxygen−oxygen line. At the total energy minimum (when d1 ≈ 2.8 Å), w2 ≈ 52° at all levels of theory.

For w1 < 90° (d1 > 2.7 Å), w2 should be less than −52.26°. Such a rotation moves the bonding hydrogen of a basal water molecule back toward the oxygen−oxygen line between direct neighbors and strengthens the base→top hydrogen bond. This effect would account for the shallow local minima around 3 Å.

For d1 > 3 Å the hydrogen bonds between nearest neighbors rapidly weaken, while interactions between second nearest neighbors change slowly (Figure 7). For d1 = 4.4 Å (the final point chosen) the interactions between second nearest neighbors in the base plane still account for 5.3% of the total energy. The bonding hydrogen atoms of the basal water molecules turn back into the water hexagon to reinforce the bonding interactions between second nearest neighbors in the base plane. Classical calculations at d1 = 4.4 Å showed that constraining the bonding hydrogen atoms to the oxygen−oxygen line (w2 = −52.54°, taken from the global minimum structure) has only a small effect on the total binding energy ($\Delta^{52.45°}_{50.61°}E_{HEX}$ = +0.011 kcal/mol). The average binding energy between nearest neighbors increases

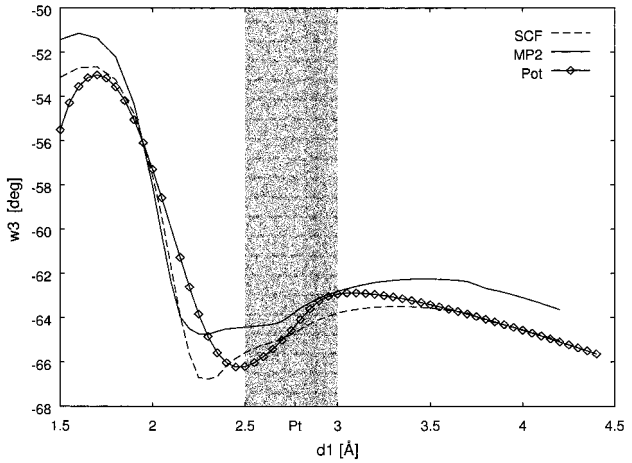

Figure 11. Angle w3 as a function of surface lattice constant d1.

by only 0.002 kcal/mol, but the binding energy between second nearest neighbors in the base plane decreases by 0.007 kcal/mol.

Figure 11 shows w3 as a function of d1, where, once again, all three curves are in reasonable agreement. The location of the first maximum suggests the formation of a water trimer in the top plane. The bonding hydrogen atoms turn into the water hexagon to form hydrogen bonds to second nearest neighbor molecules. As d1 increases, the bonding hydrogen atoms move out of the hexagon, and for d1 $\approx$ 2.2 Å, w3 reaches its theoretical optimum of $-60°$, when the bonding hydrogen atoms lie directly above the oxygen−oxygen lines and point toward the center of the basal oxygen atoms. As d1 increases further, the bonding hydrogen atom moves outside the hexagon. An analysis of the classical curve shows that this effect strengthens both base→top and top→base hydrogen bonds by reducing the hydrogen−hydrogen repulsion. At the minimum of the classical curve (d1 = 2.5 Å, w3 = $-66.2°$), the rotation of w3 back toward the oxygen−oxygen line reduces the total energy by about 0.45 kcal/mol. The increase in binding energy of 30.64 kcal/mol within the cluster is counteracted by an increase in repulsive energy of 31.09 kcal/mol. Only the interactions between second nearest (and further) neighbors benefit from this rotation, whereas the hydrogen bonds between nearest neighbors weaken because of hydrogen−hydrogen repulsions. A similar distortion has been observed at the global minimum of the water trimer, where the repulsions between nonbonding hydrogens on the same side of the oxygen triangle force the nonbonding hydrogen atoms out of the plane.

As d1 increases further, the hydrogen atoms move back inside the hexagon until the direct hydrogen bonds become strongest at d1 = 3 Å (Figure 7), when w3 decreases again, strengthening the hydrogen bonds between nearest neighbors.

5.5. Discussion. In all cases, the transition from the classical potential to MP2 via RHF resulted in a reduction in the length of the hydrogen bond and an increase in binding energy. These effects arise from the inclusion of electron correlation in the quantum calculations, whereas those of the classical potential depend strongly on the parametrization of the potential. The potential parametrized using the BSSE corrected MP3 results extends the hydrogen bond and reduces the binding energy. To detect differences between classical and quantum calculations, we consider the sequence $(H_2O)_2 \rightarrow (H_2O)_3 \rightarrow (H_2O)_6$ rather than the sequence classical potential → RHF → MP2.

As the cluster size is increased, the quantum calculations predict shorter oxygen−oxygen bond lengths in the free water cluster (MP2, 2.91 2.78, and 2.73 Å). Xantheas and co-workers[63,79] reported an exponential decrease in r_{OO} with increasing cluster size but showed also that the parameters of the exponential function depend on the method of calculation. The values of r_{OO} calculated with our classical potential showed little change with cluster size (specifically, 2.98, 2.91, and 2.95 Å). Tsai and Jordan[114] observed similar behavior in TIP4P calculations on water hexamers, where bond lengths ranged from 2.72 to 2.76 Å, values close to those for the water dimer (2.75 Å).[4,65,129,132] The reported binding energy of the cyclic hexamer (-44.4 kcal/mol) disagrees with our result of -35.4 kcal/mol. This difference may be explained through different strengths for an individual hydrogen bond (TIP4P, -6.24 kcal/mol; our potential, -4.90 kcal/mol). By applying a scale factor of $F_{Pot}^{TIPS}(E) = E_{DIM}^{TIPS4}/E_{DIM}^{Pot} = 1.27$ to an individual hydrogen bond yields a binding energy of -45.1 kcal/mol, in reasonable agreement with the published value.

Results derived from the classical potential depend critically upon the parametrization of the interaction potential. From Table 2, calculated scale factors for the bond length ($F_{Pot}^{MP2}(r_{OO})\} = 0.97$) and the binding energy ($F_{Pot}^{MP2}(E)\} = 1.28$) provide an indication of the role of cooperative effects within the cyclic hexamer at MP2 level, leading to an oxygen−oxygen bond length of 2.86 Å and a binding energy of -45.3 kcal/mol. These results suggest that many body−body effects account for -8.6 kcal/mol (16% of the total binding energy). [Our RHF calculations of multi-center energies within the constrained hexamer showed that cooperative forces account for 20% of E_{HEX} at the global minimum (d1 = 2.80 Å).] Pedulla et al.[120] reported a value of -13.48 kcal/mol (32%) for the three-, four-, five-, and six-body forces in the cyclic water hexamer, which is similar in magnitude but twice as large as a percentage of the total energy. For the cage and prism structures, many-body forces account for 22% of the total binding energy (-9.5 kcal/mol). These results can be accounted for by the higher number of hydrogen bonds in the three-dimensional clusters (cage, 8; prism, 9).

The calculations on the water hexamer agree reasonably well for all levels of theory, allowing us to discount further systematic errors. Energy differences between different configurations and the geometry of the cluster itself appear to be reasonably well defined.

As can be seen from Table 5, which contains data on the water hexamer as part of ice Ih, our calculations fail to reproduce the value of the surface lattice constant (d1) of ice. Although d1 does decline at increasing levels of theory, the limiting value of 2.6 Å is never reached. Because d1 is large, the corresponding values of d2 and w1 are small in order to create strong direct hydrogen bonds with optimal oxygen−oxygen separations.

In an extended ice crystal, w1 is controlled by the water layer below the hexamer. This basic hydrogen bond raises the hydrogens of the base molecules, thereby increasing the height of the ring. Our model does not contain such directional forces, and the water hexamer becomes more compressed than in bulk ice Ih. The oxygen−oxygen distance calculated at the MP2 level (2.74 Å) is close to that found in ice (2.76 Å). To maintain this value, an upward motion of the basal hydrogens would result in smaller values for d1. The inability of our model to reproduce d1 seems to be more a product of the finite spatial extent of the ice microcrystal than of the chosen method of computation.

Quantum calculations on the platinum−water interface[4] showed the reorientational energy $\Delta_{UP}E$ of the hydrogens to be very small ($\Delta_{UP}E < 0.5$ kcal/mol). A model with no directional forces would appear to be more realistic as a first approximation than one with strong directional forces as in ice.

Our calculations suggest that the formation of planar hexamers on hexagonal metal surfaces is feasible over a wide range of values of surface lattice constants and, by implication, of metals. As the value of the surface lattice constant d1 approaches 2.7 Å, the ring tends to planarity ($h \approx 0$; Figure 8) when the nonbonding hydrogens in the top layer are forced to point upward. A planar water hexamer in the first bilayer does not prohibit the growth of ice clusters on any surface.

As *h* decreases, the basal hydrogens move closer to the surface. For d1 ≈ 2.7 Å, w1 equals 90° and tends to 75° as d1 increases. Values of w1 smaller than 90° are unlikely to be observed in practice, because the water−metal bond is generally formed through the lone pair of the water molecule.[1,4,26]

The energy required to reorientate the water molecule in the range 90° ≤ w1 ≤ 180° is small ($\Delta_{UP}E$ = 0.26 kcal/mol for Pt_5-H_2O[4]), whereas it is energetically unfavorable to bring w1 < 90° when $\Delta_{DOWN}E$ = 35.29 kcal/mol. This energy reflects the breaking of the platinum−oxygen bond, but this does not form part of our surface model. A more elaborate surface model to account for $\Delta_{DOWN}E$ should yield a value of 90° for w1 for d1 around 2.6 Å, because the energy gain within the water hexamer caused by the downward motion of the hydrogens would be compensated by the energy necessary to distort the surface−water bond.

The possibility of the water molecules pointing downward depends on $\Delta_{DOWN}E$ and therefore on the chosen model of computation. Spohr[130,131] has published molecular dynamics simulations on the Pt(100)−water and Hg(111)−water interfaces. His simulations predict that the molecular planes of the water molecules in the first layer lie parallel to the metal surface, which agrees well with our results. In the Hg(111)−water interface, the oxygen−hydrogen bonds point toward the metal surface. Our calculations suggest that for values of d1 ≥ 2.7 Å the dipole moment vector of the water molecule should point toward the surface. The mercury−mercury separation is about 3.0 Å, and the orientation of the hydrogen atoms agrees with our results. These molecular dynamics simulations suggest that the structure of the water−metal interface might be controlled by the surface lattice constant d1, in agreement with our assumptions.

The large value for $\Delta_{DOWN}E$ suggests w1 ≥ 90°, whereas the value of w1 for a single water molecule depends on the choice of metal cluster and the method of calculation (Pt, 93.7° ≤ w1 ≤ 180°,[4] 90°,[14] 180°,[17] 90° (coadsorbed with K),[15] 180°,[18] 90°,[16] 180°;[19] Ni, 155°,[20] 180°;[24] Cu, 120°;[21] Ru, 180°;[22] Al, 125°[26]). The energy required to move the hydrogens upward $\Delta_{UP}E$ is generally small, with the exception of Pt_{10} ($\Delta_{UP}E$ < 0.5 kcal/mol;[4] Pt_{10}, ≈ 4 kcal/mol;[15,16] Ni, 0.9 kcal/mol[20] and 1.5−0.07 kcal/mol;[24] Al, 2.3 kcal/mol[26]).

Two mechanisms may be postulated for the formation of extended water clusters on metal surfaces with large values surface lattice constant:

1. The molecular plane of the water molecule lies parallel to the metal surface, even at low surface coverages such as for Pt, when the planar water hexamer can grow unhindered.

2. A single water molecule adsorbs with w1 > 90° (e.g., Ru[22] and Ni[20]). The structure of the hexamer is now determined by the energy required to distort the surface−water bond ($-\Delta_{UP}E$) and the energy gained by the downward motion of the hydrogen in the basal plane. The small values for $\Delta_{UP}E$ and the large energies for conformational changes within the water cluster reported here suggest that the water hexamer will dominate the structure of the interface, forcing the hydrogens toward the surface.

TABLE 6: Multilayer Peaks Data from Refs 1, 12, and 128

surface	d1 [Å]	ltm [Å]	*T* [K]	E_{HEX}^{MP2} [a] [kcal mol^{-1}]
Ni(111)	2.49	+0.19	170	−46.525
Cu(111)	2.56	+0.08	150	−48.128
Rh(111)	2.69	−0.16	190	−49.530
Ru(0001)	2.71	−0.19	212−220	−49.662
Re(0001)	2.76	−0.28	180	−49.562
Pt(111)	2.77	−0.30	170	−49.484
Ag(111)	2.89	−0.50	150	−47.721

[a] Extrapolated from the MP2 potential-energy curve (Figure 6).

Both possibilities generate a planar water hexamer on the surface, and this would seem likely on a hexagonal metal surface irrespective of the values of w1 found in geometry optimizations of small clusters.

Our results suggest that the direct formation of a metal−ice interface can be observed on metals with strong metal−water bonds resulting in large values for $\Delta_{UP}E$, which force the base water molecules into a suitable orientation, or for small surface lattice constants.

The influence of the surface lattice constant d1 on the binding energy of the water molecule can be seen in a plot[1,12] of the lattice mismatch ltm (distance between second nearest neighbors, ltm = Δd1$\sqrt{3}$) versus the highest desorption temperature of water from metal surfaces (multilayer peak). From Table 6, the highest desorption temperature is found for Ru(0001) (ltm = −0.19 Å, d1 = 2.71 Å) lying between 212 and 220 K.[12] If ice is assumed to grow epitaxially on a metal surface, the highest desorption temperature for the multilayer peak should be found for copper (d1 = 2.56 Å, ltm = +0.08 Å), which is closest to the bulk ice surface lattice value (d1 = 2.6 Å). The experimental multilayer desorption temperature on Cu(111) is exceptionally low (150 K). Table 6 shows that E_{HEX}^{MP2} correlates with the multilayer desorption temperature reasonably well for all values of surface lattice constants, suggesting that the true bilayer structure lies closer to the constrained hexamer (as reported here) than to bulk ice Ih.

We find that the water hexamer remains planar ($h \approx 0$) at d1 = 2.7 Å, in agreement with the experiment,[3] and suggests that the orientational forces of ruthenium on the water molecule are smaller than those of the stretched water ring. This experimental value for *h*[3] suggests that our simple model seems to reproduce both the energy and the structure of the water bilayer.

The binding energy of a single water molecule to metal surfaces (e.g., Pt, Rh, Re, Ni, and Ru[1]) is similar to the sublimation energy of ice (≈ 14 kcal/mol),[1,11,126] which corresponds to that of two to three hydrogen bonds (Table 2). A total binding energy of approximately 42 kcal/mol for three water−metal bonds can compensate for any hexamer conformation calculated here (Figure 6), but the experimentally observed range is much smaller.

In the initial stage of growth, a water molecule has two possible adsorption sites: one attached directly above a platinum and another to a water molecule already bound to the surface.[30,31] The coexistence of both species is commonly explained in terms of the energy of isolated bonds, although the importance of cooperative forces has been proposed.[11,13,133] The strength of the platinum−water bond corresponds to that of two to three hydrogen bonds, so either type of bonding should be possible.

The analysis of the classical binding energy showed that the strongest bond between a top water molecule and the remaining water pentamer (ΔE_{TOP}) can be observed close to the global maximum of the total energy (d1 = 2.95 Å, ΔE_{TOP} = −10.862 kcal/mol). This value is smaller than the energy of water bound

directly to the surface, and two-dimensional growth of the water layer on metals should be more favorable than the formation of three-dimensional islands. Quantum chemical calculations on $Pt_3-(H_2O)_3$[11] have shown, on the other hand, that cooperative effects play an important role in the formation of small water clusters on Pt(111), and the binding energy of a top water molecule should therefore be higher than that predicted by the classical potential.

The importance of cooperative effects and electron correlation can be inferred from the binding energies of a top water molecule (ΔE_{TOP}) at the global minima of the RHF (14.558 kcal/mol) and MP2 (18.199 kcal/mol) potential curves. Although the classical potential does not predict the formation of three-dimensional clusters, the formation of such clusters is predicted by the quantum calculations.

The binding energy ΔE_{TOP} decreases rapidly as the lattice constant d1 varies. The formation of three-dimensional water clusters as observed for Pt(111)[126] is therefore limited to a small range around the global minimum. Outside this region, two-dimensional growth will dominate and water molecules in the second layer will be observed only at higher surface coverage.

The existence of the planar water hexamer suggests that the structure of the metal−water interface is not continuous, as suggested by the surface ice rules, but has its own structure. This structure is closer to ice Ih and therefore closer to the QLL than to the two-dimensional ice structures reported by Koga et al.[134,135] and Odelius et al.,[136] which have similar oxygen framework ($r_{OO} = 2.73 \pm 0.02$ Å, $h \approx 0$[134]) but differ in the orientation of the hydrogen bonds.

6. Final Conclusions

The interface phase has its origin in the boundary of the ice crystal. Quantum calculations suggest that a single water molecule is bound more strongly to a metal surface (≈ 15 kcal/mol) than to the ice cluster, but the platinum−water bond, for example, has only a small influence on the orientation of the base water molecules ($\Delta_{UP}E \approx 0.5$ kcal/mol). The absence of these orientating forces allows the hydrogens of the water molecules directly attached to the metal to move freely. This free motion of the hydrogens makes the interfacial region similar to the ice−vacuum interface. The value of the lattice constant d1 seems to control the properties of the interfacial phase. As d1 increases, the water hexamer becomes flatter and the molecular plane of the base water molecules lies parallel to the metal surface. We, therefore, propose the formation of an interfacial layer as the basis for ice growth on metals other than platinum with weak orientating forces and large interatomic separations.

Acknowledgment. TL would like to thank K. Nagorny for his support and students who participated on the project: Axel Wichman, Sonja Staack, and Ingo Reulecke. He would also like to thank the Studienstiftung des Deutschen Volkes and the Hansische Universitätsstiftung for financial support.

References and Notes

(1) Thiel, P. A.; Madey, T. E. *Surf. Sci. Rep*. **1987**, *7*, 211−385.
(2) Ranke, W. *Surf. Sci*. **1989**, *209*, 57−76.
(3) Materer, N.; Starke, U.; Barbieri, A.; Van Hove, M. A.; Somorjai, G. A.; Kroes, G.-J.; Minot, C. *J. Phys. Chem*. **1995**, *99*, 6267−6269.
(4) Lankau, T. *A Computational Chemistry Analysis of the Platinum−Water−Vacuum Interface*, Ph.D. Thesis, University of Hamburg, 2000.
(5) Firment, L. E.; Somorjai, G. A. *Chem. Phys*. **1975**, *63*, 1037−1038.
(6) Firment, L. E.; Somorjai, G. A. *Surf. Sci*. **1976**, *55*, 413−426.
(7) Doering, D. L.; Madey, T. E. *Surf. Sci*. **1982**, *123*, 305−307.
(8) Bernal, J. D.; Fowler, R. H. *J. Chem. Phys*. **1933**, *1*, 515−546.
(9) Pauling, L. *J. Am. Chem. Soc*. **1935**, *57*, 2680−2684.
(10) Thiel, P. A.; Hoffmann, F. M.; Weinberg, W. H. *J. Chem. Phys*. **1981**, *75*, 5556−5572.
(11) Lankau, T.; Nagorny, K.; Cooper, I. L. *Langmuir* **1999**, *15*, 7308−7315.
(12) Hoffmann, W. *Wasseradsorptionsstrukturen auf Ru(0001) und vizinalen Rutheniumoberflächen*, Ph.D. Thesis, University of Hamburg, 1999.
(13) Langenbach, E.; Spitzer, A.; Lüth, H. *Surf. Sci*. **1984**, *147*, 179−190.
(14) Morgenstern, M.; Müller, J.; Michely, T.; Cosma, G. *Z. Phys. Chem*. **1997**, *198*, 43−72.
(15) Bonzel, H. P.; Pirug, G.; Müller, J. E. *Phys. Rev. Lett*. **1987**, *58*, 2138−2141.
(16) Müller, J. E. *Appl. Phys. A* **1989**, *49*, 681−690.
(17) Holloway, S.; Bennemann, K. H. *Surf. Sci*. **1980**, *101*, 327−333.
(18) Estiu, G.; Maluendes, S. A.; Castro, E. A.; Arvia, A. J. *J. Phys. Chem*. **1988**, *92*, 2512−2516.
(19) Anderson, A. B *Surf. Sci*. **1981**, *105*, 159−176.
(20) Yang, H.; Whitten, J. L. *Surf. Sci*. **1989**, *223*, 131−150.
(21) Ribarsky, M. W.; Luedtke, W. D.; Landman, U. *Phys. Rev. B* **1985**, *32*, 1430−1433.
(22) Khanra, B. C. *Chem. Phys. Lett*. **1981**, *84*, 107−110.
(23) Anderson, A. B.; Ray, N. K. *J. Phys. Chem*. **1982**, *86*, 488−494.
(24) Bauchlicher, C. W. *J. Chem. Phys*. **1985**, *83*, 3129−3133.
(25) Müller, J. E. *Phys. Rev. Lett*. **1984**, *53*, 2493−2496.
(26) Müller, J. E. *Surf. Sci*. **1986**, *178*, 589−607.
(27) Kuznetsov, An. M.; Nazmutdinov, R. R.; Shapnik, M. S. *Electrochim. Acta* **1989**, *34*, 1821−1828.
(28) Griffiths, K.; Bonnet, D. *Surf. Sci*. **1986**, *177*, 169−190.
(29) Kiskinova, M.; Pirug, G.; Bonzel, H. P. *Surf. Sci*. **1985**, *150*, 319−338.
(30) Fisher, G. B.; Gland, J. L. *Surf. Sci*. **1980**, *94*, 446−455.
(31) Sexton, B. A. *Surf. Sci*. **1980**, *94*, 435−445.
(32) Miller, J. N.; Lindau, I.; Spicer, W. E. *Surf. Sci*. **1981**, *111*, 595−608.
(33) Madey, T. E.; Yates, J. T., Jr. *Chem. Phys. Lett*. **1977**, *51*, 77−83.
(34) Fischer, G. B.; Sexton, B. A. *Phys. Rev. Lett*. **1980**, *44*, 683−686.
(35) Creighton, J. R.; White, J. M. *Surf. Sci*. **1982**, *122*, L648 − L652.
(36) Creighton, J. R.; White, J. M. *Surf. Sci*. **1984**, *136*, 449−462.
(37) Mooney, C. E.; Anderson, L. C.; Lunsford, J. H. *J. Phys. Chem*. **1993**, *97*, 2505−2506.
(38) Furukawa, Y. *Chem. Unserer Zeit*. **1997**, *31*, 58−65.
(39) Dosch, H.; Lied, A.; Bilgram, J. H. *Surf. Sci*. **1995**, *327*, 145−164.
(40) Kroes, G.-J. *Surf. Sci*. **1992**, *275*, 365−382.
(41) Morokuma, K.; Pedersen, L. *J. Chem. Phys*. **1968**, *48*, 3275−3282.
(42) Chen, H.-Y.; Sheu, W.-S. *J. Chem. Phys*. **1999**, *110*, 9032−9038.
(43) Kim, K. S.; Mhin, B. J.; Choi, U.-S.; Lee, K. *J. Chem. Phys*. **1992**, *97*, 6649−6662.
(44) Feller, D. *J. Chem. Phys*. **1992**, *96*, 6104−6114.
(45) van Duijneveldt-van de Ridjt, J. G. C. M.; van Duijneveldt, F. B. *J. Chem. Phys*. **1992**, *97*, 5019−5030.
(46) Honegger, E.; Leutwyler, S. *J. Chem. Phys*. **1988**, *88*, 2582−2595.
(47) Del Bene, J.; Pople, J. A. *J. Chem. Phys*. **1970**, *52*, 4858−4866.
(48) Del Bene, J.; Pople, P. A. *J. Chem. Phys*. **1973**, *58*, 3605−3608.
(49) Kistenmacher, H.; Lie, G. C.; Popkie, H.; Clementi, E. *J. Chem. Phys*. **1974**, *61*, 546−541.
(50) Popkie, H.; Kistenmacher, H.; Clementi, E. *J. Chem. Phys*. **1973**, *59*, 1325−1336.
(51) Saebø, S.; Pulay, P. *J. Chem. Phys*. **1988**, *88*, 914−922.
(52) Matsuoka, O.; Clementi, E.; Yoshimine, M. *J. Chem. Phys*. **1976**, *64*, 1351−1361.
(53) Chakravotry, S. J.; Davidson, E. R. *J. Phys. Chem*. **1993**, *97*, 6373−6383.
(54) Hankins, D.; Moskowitz, J. W.; Stillinger, F. H. *J. Chem. Phys*. **1970**, *53*, 4544−4554.
(55) Yoon, B. J.; Morokuma, K.; Davidson, E. R. *J. Chem. Phys*. **1985**, *83*, 1223−1231.
(56) Frisch, M. J.; Del Bene, J. E.; Binkley, J. S.; Schaefer, H. F., III *J. Chem. Phys*. **1986**, *84*, 2279−2289.
(57) Alagona, G.; Ghio, C.; Cammi, R.; Tomasi, J. *Int. J. Quantum Chem*. **1987** *32*, 207−226.
(58) Alagona, G.; Ghio, C.; Cammi, R.; Tomasi, J. *Int. J. Qunatum Chem*. **1987** *32*, 227−248.
(59) Newton, M. D.; Kestner, N. R. *Chem. Phys. Lett*. **1983**, *94*, 198−201.
(60) Saebø, S.; Tong, W.; Pulay, P. *J. Chem. Phys*. **1993**, *98*, 2170−2175.

(61) Yamabe, S.; Morokuma, K. *J. Am. Chem. Soc.* **1975**, *97*, 4458−4465.
(62) Umeyama, H.; Morokuma, K. *J. Am. Chem. Soc.* **1977**, *99*, 1316−1332.
(63) Xantheas, S. S.; Dunning, T. H., Jr. *J. Chem. Phys.* **1993**, *99*, 8774−8792.
(64) BNS, ST2, and Row: Stillinger, F. H.; Rahman, A. *J. Chem. Phys.* **1974**, *60*, 1545−1557.
(65) SPC, BF, TIPS2, TIP3P, and TIP4P: Jorgensen, W. L.; Chandrasekhar, J.; Madura, J. D.; Impey, R. W.; Klein, M. L. *J. Chem. Phys.* **1983**, *79*, 926−935.
(66) TIPS: Jorgensen, W. L. *J. Chem. Phys.* **1982**, *77*, 4156−4163.
(67) SPC/E: Berendsen, H. J. C.; Grigera, J. R.; Straatsma, T. P. *J. Phys. Chem.* **1987**, *91*, 6269−6271.
(68) Mas, E. M.; Szalewicz, K. *J. Chem. Phys.* **1996**, *104*, 7606−7614.
(69) Feyereisen, M. W.; Feller, D.; Dixon, D. A. *J. Phys. Chem.* **1996**, *100*, 2993−2997.
(70) Scheiner, S. *Annu. Rev. Phys. Chem.* **1994**, *45*, 23−56.
(71) Fellers, R. S.; Leforestier, C.; Braly, L. B.; Brown, M. G.; Saykally, R. J. *Science* **1999**, *284*, 945−948.
(72) Schütz, M.; Bürgi, T.; Leutwyler, S.; Bürgi, H. B. *J. Chem. Phys.* **1993**, *99*, 5228−5238. Erratum. *J. Chem. Phys.* **1994**, *100*, 1780.
(73) Lentz, B. R.; Scheraga, H. A. *J. Chem. Phys.* **1973**, *58*, 5296−5308.
(74) Nielsen, I. M. B.; Seidl, E. T.; Janssen, C. L. *J. Chem. Phys.* **1999**, *110*, 9435−9442.
(75) Engdahl, A.; Nelander, B. *J. Chem. Phys.* **1987**, *86*, 4831−4837.
(76) Coker, D. F.; Miller, R. E.; Watts, R. O. *J. Chem. Phys.* **1985**, *82*, 3554−3562.
(77) Xantheas, S. S.; Dunning, T. H., Jr. *J. Chem. Phys.* **1993**, *98*, 8037−8040.
(78) Xantheas, S. S. *J. Chem. Phys.* **1994**, *100*, 7523−7534.
(79) Xantheas, S. S. *J. Chem. Phys.* **1995**, *102*, 4505−4517.
(80) Klopper, W.; Schütz, M.; Lüthi, H. P.; Leutwyler, S. *J. Chem. Phys.* **1995**, *103*, 1085−1098.
(81) van Duijneveldt-van de Ridjt, J. G. C. M.; van Duijneveldt, F. B. *Chem. Phys.* **1993**, *175*, 271−281.
(82) Fowler, J. E.; Schaefer, H. F. *J. Am. Chem. Soc.* **1995**, *117*, 446−452.
(83) Mó, O.; Yáñez, M.; Elguero, J. *J. Chem. Phys.* **1992**, *97*, 6628−6638.
(84) Fröchtenicht, R.; Kaloudis, M.; Koch, M.; Huisken, F. *J. Chem. Phys.* **1996**, *105*, 6128−6140.
(85) Liu, K.; Elrod, M. J.; Loeser, J. G.; Cruzan, J. D.; Pugliano, N.; Brown, M. G.; Rzepiela, J.; Saykally, R. *J. Faraday Discuss.* **1994**, *97*, 35−41.
(86) Owicki, J. C.; Shipman, L. L.; Sheraga, H. A. *J. Phys. Chem.* **1994**, *79*, 1794−1811.
(87) Liu, K.; Cruzan, J. D.; Saykally, R. J. *Science* **1996**, *271*, 929−933.
(88) Wales, D. J. *Science* **1996**, *271*, 925−929.
(89) Gregory, J. K.; Clary, D. C. *J. Chem. Phys.* **1995**, *102*, 7871−7829.
(90) Gregory, J. K.; Clary, D. C. *J. Chem. Phys.* **1995**, *103*, 8924−8930.
(91) Pugliano, N.; Saykally, R. J. *Science* **1992**, *257*, 1937−1940.
(92) van Duijneveldt-van de Ridjt, J. G. C. M.; van Duijneveldt, F. B. *Chem. Phys. Lett.* **1995**, *237*, 560−567.
(93) Chałasiński, G.; Szczęśniak, M. M.; Cieplak, P.; Scheiner, S. *J. Chem. Phys.* **1991**, *94*, 2873−2883.
(94) Tachikawa, M.; Iguchi, K. *J. Chem. Phys.* **1994**, *101*, 3062−3072.
(95) Rodriguez, J.; Laria, D.; Marceca, E. J.; Estrin, D. A. *J. Chem. Phys.* **1999**, *110*, 9039−9047.
(96) Brown, M. G.; Keutsch, F. N.; Saykally, R. J. *J. Chem. Phys.* **1998**, *109*, 9645−9647.
(97) Cruzan, J. D.; Braly, L. B.; Liu, K.; Brown, M. G.; Saykally, R. J. *Science* **1996**, *271*, 59−62.
(98) Liu, K.; Brown, M. G.; Saykally, J. R. **1996**, *271*, 62−64.
(99) Loerting, T.; Liedl, K. R.; Rode, B. M. *J. Chem. Phys.* **1998**, *109*, 2672−2679.
(100) Corrales, L. R. *J. Chem. Phys.* **1999**, *110*, 9071−9080.
(101) Merrill, G. N.; Gordon, M. S. *J. Phys. Chem. A* **1998**, *102*, 2650−2657.
(102) Wales, D. J.; Walsh, T. R. *J. Chem. Phys.* **1997**, *106*, 7193−7207.
(103) Brudermann, J.; Melzer, M.; Buck, U.; Kazimirzki, J. K.; Sadlej, J.; Bush, V. *J. Chem. Phys.* **1999**, *110*, 10649−10652.
(104) Buck, U.; Ettischer, I.; Melzer, M.; Bush, V.; Sadlej, J. *Phys. Rev. Lett.* **1998**, *80*, 2578−2581.
(105) Jiang, J. C.; Chang, J.-C.; Wang, B.-C.; Lin, S. H.; Lee, Y. T.; Chang, H.-C. *Chem. Phys. Lett.* **1998**, *289*, 373−382.
(106) Nigra, P.; Kais, S. *Chem. Phys. Lett.* **1999**, *305*, 433−438.
(107) McDonald, S.; Ojamäe, L.; Singer, S. J. *J. Phys. Chem. A* **1998**, *102*, 2824−2831.
(108) Burnham, C. J.; Li, J.; Xantheas, S. S.; Leslie, M. *J. Chem. Phys.* **1999**, *110*, 4566−4581.
(109) Kim, J.; Majumdar, D.; Lee, H. M.; Kim, K. S. *J. Chem. Phys.* **1999**, *110*, 9128−9134.
(110) Wales, D. J.; Hodges, M. P. *Chem. Phys. Lett.* **1998**, *286*, 65−72.
(111) Gregory, J. K.; Clary, D. C. *J. Phys. Chem.* **1996**, *100*, 18014−18022.
(112) Kim, J.; Kim, K. S. *J. Chem. Phys.* **1998**, *109*, 5886−5895.
(113) Mhin, B. J.; Kim, J.; Lee, S.; Kim, K. S. *J. Chem. Phys.* **1994**, *100*, 4484−4486.
(114) Tsai, C. J.; Jordan, K. D. *Chem. Phys. Lett.* **1993**, *213*, 181−188.
(115) Mhin, B. J.; Kim, H. S.; Kim, H. S.; Yoon, C. W.; Kim, K. S. *Chem. Phys. Lett.* **1991**, *176*, 41−45.
(116) Schulson, E. M. *JOM 51*, **1999**, 21−27.
(117) Belch, A. C.; Rice, S. A. *J. Chem. Phys.* **1987**, *86*, 5676−5682.
(118) Liu, K.; Brown, M. G.; Carter, C.; Saycally, R. J.; Gregory, J. K.; Clary, D. C. *Nature* **1969**, *381*, 501−503.
(119) Nauta, K.; Miller, R. E. *Science* **2000**, *287*, 293−295.
(120) Pedulla, J. M.; Kim, K.; Jordan, K. D. *Chem. Phys. Lett.* **1998**, *291*, 78−84.
(121) Benedict, W. S.; Gailar, N.; Plyer, E. K. *J. Chem. Phys.* **1956**, *24*, 1139−1165.
(122) GAMESS−UK, Guest, M. F.; van Lenthe, J. H.; Kendrick, J.; Schoffel, K.; Sherwood, P.; Harrison, R. J.; with contributions from Amos, R. D.; Buenker, R. J.; Dupuis, M.; Handy, N. C.; Hillier, I. H.; Knowles, P. J.; Bonacic-Koutecky, V.; von Niessen, W.; Saunders, V. R.; Stone, A. J. The package is derived from the original GAMESS code by Dupuis, M.; Spangler, D.; Wendoloski, J. NRCC Software Catalog, Vol. 1, Program No. QG01 *GAMESS*, 1980.
(123) Dunning, T. H., Jr. *J. Chem. Phys.* **1970**, *53*, 2823−2833.
(124) Boys, S. F.; Bernardi, F. *Mol. Phys.* **1970**, *19*, 553−556.
(125) Frisch, M. J.; Trucks, G. W.; Schlegel, H. B.; Gill, P. M. W.; Johnson, B. G.; Robb, M. A.; Cheeseman, J. R.; Keith, T.; Petersson, G. A.; Montgomery, J. A.; Raghavachari, K.; Al-Laham, M. A.; Zakrzewski, V. G.; Ortiz, J. V.; Foresman, J. B.; Cioslowski, J.; Stefanov, B. B.; Nanayakkara, A.; Challacombe, M.; Peng, C. Y.; Ayala, P. Y.; Chen, W.; Wong, M. W.; Andres, J. L.; Replogle, E. S.; Gomperts, R.; Martin, R. L.; Fox, D. J.; Binkley, J. S.; Defrees, D. J.; Baker, J.; Stewart, J. P.; Head-Gordon, M.; Gonzalez, C.; Pople, J. A. *Gaussian 94*, revision C.2; Gaussian, Inc.: Pittsburgh, PA, 1995.
(126) Ogasawara, H.; Yoshinobu, J.; Kawai, M. *Chem. Phys. Lett.* **1994**, *231*, 188−192.
(127) Brudermann, J.; Lohbrandt, P.; Buck, U.; Buch, V. *Phys. Rev. Lett.* **1998**, *80*, 2821−2824.
(128) WebElements Pro—The periodic table on the World Wide Web; www.webelements.com.
(129) Wilson, M. A.; Pohorille, A.; Pratt, L. R. *J. Phys. Chem.* **1987**, *91*, 4873−4878.
(130) Spohr, E.; *Computer Simulation of the Structure and Dynamics of Water Near Metal Surfaces*; Solid−Liquid Electrochemical Interfaces; ACS Symposium Series 656; American Chemical Society: Washington, DC, 1997; Chapter 3, pp 32−44.
(131) Spohr, E. Computer Modelling of Aqueous/Metallic Interfaces; Habilitationsschrift University Ulm, **1995**.
(132) Wilson, M. A.; Pohorille, A.; Pratt, L. R. *J. Phys. Chem.* **1988**, *88*, 3281−3285.
(133) Miller, J. N.; Ling, D. T.; Stefan, P. M.; Weissman, D. L.; Shek, M. L.; Lindau, I.; Spicer, W. W. *Phys. Rev. B.* **1981**, *24*, 1917−1926.
(134) Koga, K.; Zeng, X. C.; Tanaka, H. *Phys. Rev. Lett.* **1997**, *79*, 5262−5265.
(135) Tanaka, H.; Yamamoto, R.; Koga, K.; Zeng, X. C. *Chem. Phys. Lett.* **1999**, *304*, 378−384.
(136) Odelius, M.; Bernasconi, M.; Parinello, M. *Phys. Rev. Lett.* **1997**, *78*, 2855−2858.
(137) Dyke, T. R.; Muenter, J. S. *J. Chem. Phys.* **1974**, *60*, 2929−2930.
(138) Curtiss, L. A.; Frurip, D. J.; Blander, M. *J. Chem. Phys.* **1979**, *71*, 2703−2711. This article provides the experimental data used by Kim et al.[43] and others for the calculation of the dimerisation energy.